

RADIATIVE TRANSFER CODE COMPARISON FOR MERIS VICARIOUS CALIBRATION

R. Santer⁽¹⁾, F. Zagolski⁽²⁾, and E. Dilligeard⁽³⁾

⁽¹⁾ LISE/MREN, Université du Littoral Côte d'Opale, 32 Avenue Foch, Wimereux, F62930 – FRANCE,
E-mail: santer@mren2.univ-littoral.fr

⁽²⁾ PRIVATEERS N.V., Great Bay Marina, Philipsburg – NETHERLANDS-ANTILLES,
PARBLEU Technologies Inc., 570 Charest-Est, Suite #511, Quebec (Qc) – CANADA G1K-9G3,
E-mail: Francis_Zagolski@hotmail.com

⁽³⁾ HYGEOS SCOP, 191 rue Nicolas Appert, Villeneuve d'Ascq F59650 – FRANCE,
E-mail: ed@nerim.net

ABSTRACT

Different groups are involved in the MERIS vicarious activities. Most of the time, the prediction of the incoming radiance to the sensor needs radiative transfer computations. An inter comparison exercise is reported here based on radiative transfer computations with different codes applied on suitable test cases for vicarious calibration. Because the top of atmosphere signal over bright targets mostly depends upon the surface reflectance, a good agreement appears for vicarious calibration over land. Over the dark ocean, first, there is a need to account for the polarization mostly for the molecular scattering. Second, large discrepancies result from the computation of the aerosol scattering which have to be more deeply understood.

1. INTRODUCTION

The physical interpretation of satellite data needs an accurate sensor calibration. An accuracy of few percents is required for the radiometric calibration of ocean color missions. The calibration protocol usually includes a pre-launch radiometric activity as well as an onboard checking [1]. In that purpose some of the ocean color sensors, such as MERIS (MEdium Resolution Imaging Spectrometer) and SeaWiFS (Sea-viewing Wide Field of view Sensor), are equipped with diffuser panels to measure the solar irradiance on a daily basis [2]. Nevertheless, it is difficult to separate the degradation of the sensor calibration from a change in a panel reflectance. The lunar [3] has then been used as well for the SeaWiFS sensor in order to indicate variations in the panel characteristics. This technique is based on the assumption that the moon is a diffuse reflector whose the surface remains radiometrically stable. The sensor points on the moon monthly in order to evaluate the temporal degradation of its sensitivity for each channel [4]. For MERIS, it is foreseen to employ a twin panel: one is deployed occasionally (to avoid degradation in the space environment) to cross check with the panel routinely used. The cross calibration between sensors is also often used to check the validity of the sensors sensitivity. For example, the MOS sensor was recalibrated using the SeaWiFS data [5] and POLDER (POLarization and Directionality of the Earth's Reflectance) was cross-calibrated with OCTS (Ocean Color and Temperature Scanner).

The most direct way to perform vicarious calibration is to measure the radiance in the same condition as the satellite or platform. Well calibrated radiometers can be employed on board an aircraft. This technique has been successfully tested several times over white sand surfaces [6] or over lakes [7] selected as a dark target for ocean colour sensors. However, the maximum altitude of 3 km implies to perform a residual atmospheric correction. An alternative approach, used for SeaWiFS, was to cross calibrate with AVIRIS (Airborne Visible / Infrared Imaging Spectrometer) which flies at approximately 20 km above sea level. Unfortunately, this technique is very quite expensive. A current and secure mean of calibration to provide good ocean colour products is the vicarious calibration [8] for which we need both an accurate description of the atmospheric and oceanic optical properties.

2. MERIS VICARIOUS CALIBRATION

2.1 MERIS Characteristics

Table 1 summarizes the nominal wavelength for each of the 15 MERIS bands. In the first place, we have to exclude from the vicarious calibration study the O_2 band at 760.625 nm and the H_2O band at 900 nm which present too large absorptions. Actually, these two bands are used in a differential method (respectively with 753.75 nm and with 885 nm). We can strongly believe that the required inter-calibrations 760.625/753.75 and 900/885 will be accurately achieved

using the on-board panel. For these two sets of bands, it is preferable to evocate vicarious calibration of the products. This is the case for the calibration of the surface pressure as already achieved for the MOS sensor [9]. Except for these two MERIS bands, the gaseous absorption is reduced thanks to narrow bandwidth. We mostly need to account for the O_3 absorption in the *Chapuis* band and some residual one for H_2O at 708.75nm and O_2 at 778.75nm . The O_3 absorption is well defined from the ozone amount. According to Table 1, there is very residual gaseous absorption by the water vapour (H_2O) at 708.75nm . By consistency with the level-2 products, we recommend to account for the continuum. The O_2 absorption at 778.75nm is quite minor. Because this gaseous absorption correction does not make problems, we will ignore it in the inter-comparison exercise.

Generally, the calibration equation relies the digital counts (DC) to the incoming radiance (L). This association is completed on the on-board panel. In each MERIS band i , for each pixels j , we then get a calibration coefficient $A_i(j)$ expressed as:

$$L_i^e(j) = A_i(j) \cdot DC_i(j) \quad (1)$$

where the digital counts $DC_i(j)$ recorded for band i on the pixel j correspond to $L_i^e(j)$ reflected by the spectralon as:

$$L_i^e(j) = \mu_s^i(j) \cdot \frac{E_s^i(j)}{\pi \cdot d^2} \cdot \rho_p^i(j) \quad (2)$$

which is derived from known values of the solar irradiance $E_s^i(j)$, of the panel reflectance $\rho_p^i(j)$ and of the cosine $\mu_s^i(j)$ of the incident solar angle on the panel. Vicarious calibrations are mostly based on the estimate of the top of atmosphere (TOA) reflectance. Eq. 2 also applies to the case where the smile effect should be introduced. In this inter-comparison exercise, we will not consider the smile effect and the solar irradiance will be set to $1\text{ Wm}^{-2}\text{sr}^{-1}$.

Table 1: Rayleigh (δ_R) and ozone (δ_{O_3}) optical thicknesses, and gaseous transmittivities in the 15 MERIS bands for a mid-latitude summer profile for a solar zenith angle of 30° and a nadir view. H_2O^* denotes the water vapor continuum.

Band	$\lambda(\text{nm})$	$\Delta\lambda(\text{nm})$	δ_{O_3}	δ_R	Absorbers	T_{H_2O}	T_{O_2}	T_{O_3}
1	412.5	10	$9.66 \cdot 10^{-5}$	0.314	O_3	1.0000	1.0000	0.9999
2	442.5	10	$1.05 \cdot 10^{-3}$	0.235	O_3	0.9994	1.0000	0.9990
3	490	10	$6.78 \cdot 10^{-3}$	0.155	O_3	0.9998	1.0000	0.9932
4	510	10	$1.34 \cdot 10^{-2}$	0.131	H_2O+O_3	0.9965	1.0000	0.9867
5	560	10	$3.33 \cdot 10^{-2}$	0.090	O_3	1.0000	1.0000	0.9672
6	620	10	$3.49 \cdot 10^{-2}$	0.059	O_3	1.0000	1.0000	0.9657
7	665	10	$1.64 \cdot 10^{-2}$	0.045	O_3	1.0000	1.0000	0.9838
8	681.25	7.5	$1.15 \cdot 10^{-2}$	0.041	H_2O+O_3	0.9995	1.0000	0.9886
9	708.75	10	$6.30 \cdot 10^{-3}$	0.035	H_2O+O_3	0.9675	1.0000	0.9937
10	753.75	7.5	$3.06 \cdot 10^{-3}$	0.027	$H_2O^++O_3$	0.9997	1.0000	0.9969
11	760.625	3.75	$2.34 \cdot 10^{-3}$	0.026	O_2+O_3	1.0000	0.4268	0.9977
12	778.75	15	$2.46 \cdot 10^{-3}$	0.024	$H_2O^++O_2$	0.9996	0.9985	0.9975
13	865	20	$7.02 \cdot 10^{-4}$	0.015	H_2O^*	0.9990	1.0000	0.9993
14	885	10	$3.88 \cdot 10^{-4}$	0.014	H_2O	0.9920	1.0000	0.9996
15	900	10	$4.85 \cdot 10^{-4}$	0.013	H_2O	0.7378	1.0000	0.9995

Most of the case, MERIS will not saturate over land. Consequently, vicarious calibration over bright land test sites is possible. In the full spatial resolution the ground pixel size is about 300m which offers the possibility to select several land test sites. Moreover, the field of view (FOV) of 40° reduced the bi-directionality of the target, and the diffuse contribution of the surface will be considered as lambertian.

2.2 Vicarious calibration over land

The first vicarious calibration was achieved for SPOT (Satellite Pour l' Observation de la Terre) over a land target [10]. For the SPOT-HRV sensors, the inter-calibration with the lamp (on-board calibration) is assumed to provide the relative sensitivity loss with time. In order to improve the absolute accuracy of calibration factors, data obtained from lamp measurements have to be completed with field measurements using test sites such as White Sands (New Mexico) [6] and La Crau (France) [11]. The main problems encountered in these kinds of campaigns are that they are time-consuming, they need a lot of human resources to lead one and they are subjected to atmospheric conditions. These are the reasons for which the databases acquired during these campaigns are often reduced. Thus, a practical trade-off between effort/cost and absolute calibration accuracy exists. Methods that do not require field measurements have the advantage in that they can be used retrospectively for data that have already been acquired, they require no advanced planning before calibration, and they are less expensive.

In principle, vicarious calibration associates digital counts recorded by the satellite sensor with predicted incoming radiance to the sensor. In order to assess this signal, we have to characterize both the atmosphere and the ground surface. The approach we adopted for the MERIS vicarious calibration study is the same as for the SPOT one. The latter belongs to the so-called *reflectance based calibration* and its general flowchart is depicted in Fig. 1.

- (a) There is no need to have radiometer calibrated in energy. The surface reflectance is derived from a cross comparison between the test site reflectance and the well known reflectance of a reference panel. The aerosols are characterized by non absolute values.
- (b) In each spectral band, around the time of overpass, the surface reflectances are measured over the test site. These reflectances are spatially averaged. The surface is generally assumed to be Lambertian.
- (c) The *Rayleigh* scattering depends upon the *Rayleigh* optical thickness τ_r and is proportional to the barometric pressure.
- (d) Another input is the aerosol model. The main parameter is the aerosol optical thickness τ_a measured at the satellite time of overpass. There is often a need to spectrally interpolate the ground based measurements to the satellite spectral bands. A similar approach to the *Rayleigh* scattering (see Eqs. 3-4) can then be completed using a *Junge* size distribution:

$$n(r) = \frac{dN}{dr} = C \cdot r^\nu \quad (3)$$

with ν the *Junge* parameter directly related to the *Angström* coefficient α : $\nu = \alpha - 3$ (4)

The refractive index of the particles derives from the local climatology and the particle shape is assumed to be spherical in order to apply the *Mie's* theory.

(e) Ozone amount is provided by different sources, default is the climatology. Water vapor content is generally measured at the surface level. Radio-sondes may be also available to provide a vertical atmospheric profile.

(f) A radiative transfer code (RTC) is used with the surface reflectance as boundary condition. The atmospheric inputs are the barometric pressure (to compute the *Rayleigh* scattering) and the aerosol model. Generally, a first run with the RTC is completed to compute the TOA radiance ignoring the gaseous absorption which allows then to estimate the gaseous transmittance. Scattering and gaseous absorption are decoupled. As an example, the successive order of scattering (SO) [12] method and the 6S [13] outputs can be combined to predict the incoming reflectance (normalized radiance, $E_s = \pi$) for each sensor band [14].

(g) Solar irradiances are used to get radiances.

(h) Digital counts are extracted for the test site.

(i) The calibration equation (see Eq. 1) is applied.

An alternative vicarious calibration is to use stable bright sites. The latter can be employed to perform absolute calibration as first proposed by [15] with the dune areas of White Sands. The same scheme as above is then processed. Simply, because inputs are based on climatologic values, each calibration point is less accurate than if there are field

measurements at the satellite time of overpass. This calibration is applied on routine basis in order to reduce the errors by averaging. Of course, the final accuracy deeply depends on your mean outputs. Any error on them will results in bias in the calibration coefficients. Generally, these methods are used for inter temporal calibration. Then they assume to know the TOA radiances and there is no need to run a RTC.

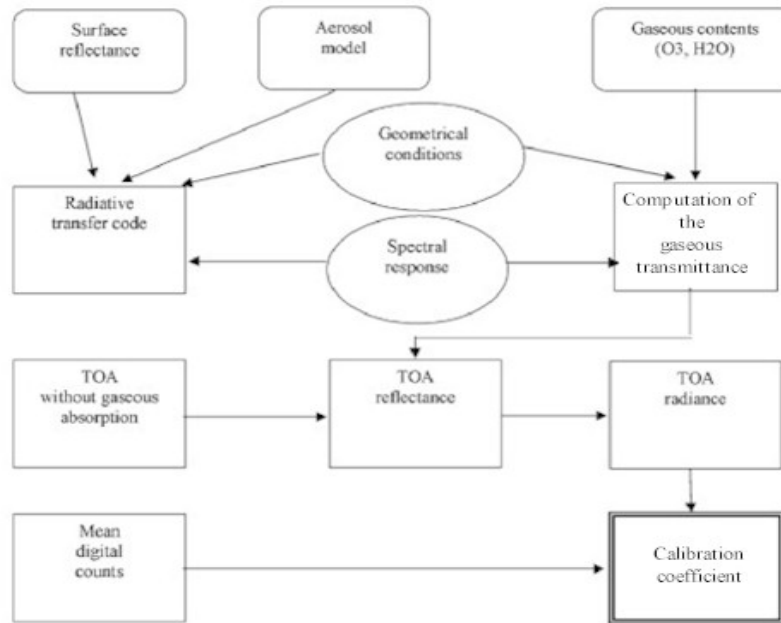


Fig. 1: Flowchart for vicarious calibration

2.3 Vicarious calibration over ocean

The same scheme as for the land can be applied to the ocean. There is a clear need for ocean colour sensors to achieve calibration over dark targets because of saturation. If the field measurements are available, the flowchart from Fig. 1 is then employed. The surface reflectances are derived from water-leaving radiances and the *Fresnel* reflection is added as boundary conditions. Naturally, the contribution of the atmospheric scattering is predominant which directly impacts on the need to have first, a well characterization of the atmospheric optical properties and second, an accurate RTC. Without field measurements, the calibration will be limited to short wavelengths to take advantage of the predominant *Rayleigh* scattering. This so called *Rayleigh* calibration needs an aerosol correction. Based on the knowledge of the inter-calibration, the aerosol information collected in the near-infrared (NIR) is reported in the visible (VIS) to complement the *Rayleigh* contribution. In terms of RTC computations, because the aerosol component is measured, it is mainly critical to correctly compute the *Rayleigh* scattering.

3. RTC COMPARISON

Four institutes participate to these inter-comparison exercise: LISE, LOA-CNES (Laboratoire d'Optique Atmosphérique, Villeneuve'Ascq - France ; Centre National d'Etudes Spatiales, Toulouse - France), LOV (Laboratoire Océanographie de Villefranche/Mer, France) and NASDA/EORC (NASDA/Earth Observation Research Center, Tokyo - Japan). Radiative transfer equation (RTE) within the coupled '*Atmosphere-Land/Ocean*' system is solved by RTC/LISE and RTC/CNES-LOA using the successive order (SO) of scattering method [12]. These two RTCs originate from the same source but with a different history. The RTC/LOV simulates the radiative transfer within the coupled '*Atmosphere/Ocean*' system using the Monte Carlo (MC) technique while the RTC/EORC (*i.e.*, the RSTAR-5b code [16]) computes the upwelling TOA radiances above a land/ocean surface using matrix formulations for a pure scattering atmosphere [17]. Due to the fact that RTC/LOV and RTC/EORC do not account for the polarization processes, a flag was activated in the RTC/LISE to unselect the polarization calculation in order to compare output upwelling radiances derived from these RTCs.

3.1 Molecules and aerosol optical properties

The first comparison brought on the *Rayleigh*. As expected, differences are negligible between the LISE, CNES-LOA and EORC derived *Rayleigh* phase function which is based on the *Travis and Hansen* formulation [18]. Residual differences remain with LOV but there are more than acceptable.

We then selected a continental model *C*: a *Junge* size distribution (see Eqs. 5-6) with $\nu=-4$ between extreme radii of $0.1\mu\text{m}$ and $20\mu\text{m}$. There is no particle with radii r larger than $20\mu\text{m}$ and if $r\leq 0.1\mu\text{m}$, the number of particles is constant. The refractive index is $m=1.45$ with an imaginary part of 0.005. Computations are conducted at 442.5nm (*C_02*) and at 865nm (*C_13*). A maritime model corresponding to larger particles ($\nu=-3.5$) made of water ($m=1.33$) was also considered in the same MERIS bands (*resp.*, *M_02* and *M_13*). These 4 test cases have been processed with each of the 4 *Mie*'s codes (LISE, LOA-CNES, LOV and EORC). The scattering phase matrices computed with the LISE *Mie*'s code have been generated with a *Gaussian* quadrature (181 angles), then linearly interpolated to be resampled with an angular step of 2 degrees between 0 and 180° which was used in the LOA-CNES *Mie*'s code. Due to the fact that the scattering phase functions computed by the two other *Mie*'s codes (LOV and EORC) have been generated with two different *Gaussian* quadratures, the LOV and EORC derived phase functions were resampled to LISE scattering angles using a linear interpolation.

We did not report here a comparison on the extinction and scattering coefficients. The agreement between the four institutes is better within four figures [19]. The discrepancies observed on the aerosol phase function mainly occur in the forward scattering for the first angle. The errors come from the difficulty to compute the forward scattering for large particles (there is more for the maritime model) and at short wavelength. The agreement in backward scattering is very satisfactory, as we can see on the mean absolute relative differences summarized in 3.1.

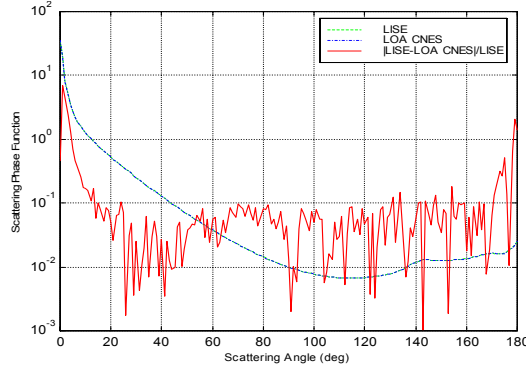


Fig. 2: Aerosol phase function at 865nm (case *M_13*) for the maritime model as computed by LISE and LOA-CNES *Mie*'s code. Because the two plots overlap, we also plot the

3.1 Over land

For the land cases, in the MERIS bands 2 (442.5nm) and 13 (865nm), we took surface reflectances respectively of 0.2 and 0.5 as representative of *Saharan* site. Solar zenith angle (SZA) was fixed to 43.61° , the maximum view zenith angle (VZA) was 40° for a scanning plan perpendicular to the solar plane (RAA= 90°). Cases l-1 and l-2 correspond to bands 2 and 13 respectively for a pure molecular atmosphere. The continental model was used for the same 2 bands in cases l-3 and l-4 with an aerosol optical thickness (AOT) respectively of 0.2 and 0.1 in bands 2 and 13.

Table 2: Comparison with LISE computations of the scattering phase function with: (a) maximum absolute difference, (b) maximum absolute relative difference (in percent) and (c) mean absolute relative difference (in percent). Absolute differences with LISE are reported for (1) CNES-LOA, (2) LOV and (3) EORC.

Case	$a1$	$a2$	$a3$	$b1$	$b2$	$b3$	$c1$	$c2$	$c3$
<i>Rayleigh</i>	$4 \cdot 10^{-5}$	$2 \cdot 10^{-4}$	$4 \cdot 10^{-4}$	0.039	0.342	0.177	0.014	0.151	0.030
<i>C_02</i>	0.682	0.680	0.015	9.327	9.306	1.925	0.151	0.384	0.758
<i>C_13</i>	0.235	0.244	0.017	3.812	3.952	1.587	0.094	0.162	0.574
<i>M_02</i>	4.002	4.025	0.045	16.617	16.715	22.032	0.244	0.346	2.508
<i>M_13</i>	1.400	1.438	0.044	6.873	7.061	14.240	0.157	1.164	2.105

Excellent agreements were observed between LISE/SO and each of the 3 other RTCs (LOA-CNES/SO, LOV/MC and EORC/RSTAR-5b) both for all the *Rayleigh* case [19]. With the continental aerosols, the discrepancies around few tenths of a percent fall within the mission requirements (see Table 3).

Table 3: Absolute and relative difference (maximum and mean values) over land cases for a SZA of 43.61° and a RAA of 90° , between (1) LISE/SO and LOA-CNES/SO (including polarization), and (2) LISE/SO and EORC/STAR-5b (without polarization): (a) maximum absolute difference, (b) maximum absolute relative difference (in percent), (c) mean absolute difference, and (d) mean absolute relative difference (in percent).

Case	a1	a2	b1	b2	c1	c2	d1	d2
l-1	10^{-5}	$5 \cdot 10^{-5}$	$7 \cdot 10^{-4}$	0.084	10^{-5}	$4 \cdot 10^{-5}$	$4 \cdot 10^{-4}$	0.077
l-2	10^{-5}	10^{-5}	10^{-4}	0.006	10^{-5}	10^{-5}	$7 \cdot 10^{-5}$	0.006
l-3	10^{-4}	$8 \cdot 10^{-5}$	0.230	0.146	10^{-4}	$8 \cdot 10^{-5}$	0.178	0.138
l-4	$7 \cdot 10^{-4}$	10^{-5}	0.639	0.007	$6 \cdot 10^{-4}$	10^{-5}	0.541	0.005

3.2 Over ocean

For the ocean cases, in the MERIS bands 2 (442.5 nm) and 13 (865 nm), surface reflectances were equal to 0.05 and 0 respectively, as representative of clear waters, for the SO inter-comparison (LISE/LOA-CNES) while a black sea surface was considered for the two other RTC-intercomparisons (*i.e.*, LISE/LOV and LISE/EORC). Moreover, the *Cox-Munk* model [20] was selected to introduce a wave slope distribution to compute the *Fresnel* reflection. RTC-intercomparisons between LISE/SO and the three other codes were performed above a wind-roughened sea surface induced by a wind speed of 7.2 m/s with (LISE/LOV and LISE/EORC) and without (LISE/LOA-CNES) accounting for the sun glint water reflectance. SO (*resp.*, MC and STAR-5b) simulations were conducted with a SZA of 43.61° (*resp.*, 45°), a maximum VZA of 40° and in the scanning plan perpendicular to the solar plane (RAA= 90°). Cases o-1 and o-2 correspond to band 2 and 13 respectively for a pure molecular atmosphere. The maritime model was used for the same 2 bands in cases o-3 and o-4 with an AOT respectively of 0.2 and 0.1 in bands 2 and 13.

Table 4 illustrates the influence of the polarization in the TOA radiance simulated with the RTC/LISE (SO) for these 4 ocean cases. A more extensive comparison stressed that the need to include the polarization processes in the TOA radiance computations is underlined mostly for the *Rayleigh* scattering [19].

Because the surface is quite dark, the discrepancies between the RTC/LISE and each of the three other RTCs are emphasized. The latter deeply exist between LISE/SO and LOA-CNES/SO (Fig. 3) and the other two codes even for the *Rayleigh* scattering. These are much higher at 865 nm in spite of the fact that we are very close to the primary scattering. By introducing the aerosols, it is worst mainly at 865 nm for which the aerosol scattering dominate (see Table 4 and Table 5).

Table 4: Absolute and relative difference (maximum and mean values) over ocean cases for a SZA of 43.61° and a RAA of 90° , (1) between LISE/SO with and without polarisation, and (2) between LISE/SO and LOA-CNES/SO including polarization: (a) maximum absolute difference, (b) maximum absolute relative difference (in percent), (c) mean absolute difference, and (d) mean absolute relative difference (in percent).

Case	a1	b1	c1	d1	a2	b2	c2	d2
o-1	$7 \cdot 10^{-4}$	2.076	$5 \cdot 10^{-4}$	1.377	$9 \cdot 10^{-5}$	0.268	$7 \cdot 10^{-5}$	0.214
o-2	$2 \cdot 10^{-5}$	1.402	10^{-5}	0.936	10^{-5}	0.445	10^{-5}	0.323
o-3	$6 \cdot 10^{-4}$	1.745	$4 \cdot 10^{-4}$	1.162	$6 \cdot 10^{-4}$	1.440	$5 \cdot 10^{-4}$	1.310
o-4	$3 \cdot 10^{-5}$	1.155	$3 \cdot 10^{-5}$	0.882	$3 \cdot 10^{-4}$	10.087	$3 \cdot 10^{-4}$	9.318

Table 5: Absolute and relative difference (maximum and mean values) over ocean cases for a SZA of 43.61° and a RAA of 90°, between (1) LISE/SO and LOV/MC and (2) LISE/SO and EORC/STAR-5b, without polarization: (a) maximum absolute difference, (b) maximum absolute relative difference (in percent), (c) mean absolute difference, and (d) mean absolute relative difference (in percent).

Case	a1	a2	b1	b2	c1	c2	d1	d2
o-1	4 10 ⁻⁴	5 10 ⁻⁴	1.604	2.211	2 10 ⁻⁴	4 10 ⁻⁴	1.034	1.724
o-2	5 10 ⁻⁵	4 10 ⁻⁴	2.656	17.160	2 10 ⁻⁵	2 10 ⁻⁴	0.993	8.401
o-3	7 10 ⁻⁴	7 10 ⁻⁴	2.703	2.811	4 10 ⁻⁴	7 10 ⁻⁴	1.487	2.481
o-4	3 10 ⁻⁴	5 10 ⁻⁴	8.940	15.273	7 10 ⁻⁵	3 10 ⁻⁴	2.090	10.728

4. CONCLUSION

This RTC-intercomparison exercise appeared unexpectedly useful. May be the errors are in the intercomparison itself (miss-understanding in the inputs) rather than in the codes. This task should be more deeply investigated with an extensive well defined data set.

The first obvious conclusion is to process the data with a RTC dealing with the polarization at least for the *Rayleigh* scattering. This recommendation is less strong for the calibration over desertic sites for which the accuracy mostly results from the determination of the surface reflectance.

Over ocean, we can accept to have differences between the RTCs on the aerosol term because the aerosol component is measured at 865 nm and transported in the *blue* region. For absolute vicarious calibration, a good accuracy (better than observed here) is required. In the lack of agreement, the recommendation is to use the same code for calibration than the one used for LUTs generation for atmospheric correction over water. We then expect that the bias in the forward mode (calibration) will be counterbalance in the backward mode (atmospheric correction).

ACKNOWLEDGEMENTS

This work has been financially supported by the European Space Agency (ESA) under the contract referred as «ESRIN-15992/02/I-LG». We first thank *Jean Paul Huot* and *Steven Delwart* from ESA and *Olivier Hagolle* from CNES for their useful comments all over this work. The authors would like specially to thank *Jean-Claude Roger* from LISE for his assistance in the use of the RTC/LISE. We also grateful to *Bruno Lafrance* and *Caroline Ruffel* from Communication Systèmes Inc. - Système d'Information (CSSI, Toulouse - France), *David Antoine* and *Bernard Gentili* from Laboratoire Océanographie de Villefranche/Mer (LOV, Villefranche/Mer - France), and *Jens Nieke*, *Wen-Zhong CHEN* and *Robert Hoeller* from Earth Observation Research Center (NASDA/EORC, Tokyo - Japan), for providing their simulations with RTC/LOA-CNES, RTC/MC and RTC/RSTAR respectively.

REFERENCES

- Gordon, H.R., Calibration requirements and methodology for remote sensors viewing the ocean in the visible, *Remote Sensing of Environment*, Vol 22,103-126, 1987.
- Barnes R.A., and Eplee R.E Jr, The SeaWiFS solar diffuser, In *R.A. Barnes, E-N. Yeh, and R.E. Eplee Jr Eds., SeaWiFS Calibration Topics, Part-1, NASA Technical Memo.-104566* (NASA/GSFC-Goddard Space Flight Center), Greenbelt (MD), Vol 39, 1703-1712, 1996.
- Kieffer H.H., and Widley R.L., Establishing the moon as a spectral radiance standard, *Journal of Atmospheric and Oceanic Technology*, Vol 13, 360-375, 1996.
- Barnes R.A., Eplee R.E. Jr, F.S. Patt, and McClain C.R., Changes in the radiometric sensitivity of SeaWiFS determined from lunar and solar-based measurements, *Applied Optics*, Vol 38,4649-4664, 1999.
- Wang M., and Franz B., Comparing the ocean color measurements between MOS and SeaWiFS: a vicarious intercalibration approach for MOS, *I.E.E.E. Transactions on Geoscience and Remote Sensing*, Vol 38 (1),184-197, 2000.

6. Thome K.J., Parada R., Schiller S., Conel J., and LaMarr J., Evaluation of the use of dark and bright targets for the in-flight calibration of AVIRIS, In *Proceedings of the 7th Annual JPL Airborne Earth Science Workshop (NASA JPL AVIRIS Workshop)*, Pasadena (CA), January 12-16, 1998.
7. Parada R., Thome K.J., and Santer R., Results of dark target vicarious calibration using lake Tahoe, In *Proceedings of the European Symposium on Aerospace Remote Sensing (SPIE Conference on Image and Signal Processing for Remote Sensing)*, EUROPTO III, Taormina (Italy), September 23-27, 1997.
8. Gordon H.R., and Zhang T., How well can radiance reflected from the ocean-atmosphere system be predicted from measurements at the sea surface, *Applied Optics*, Vol 35 (33),6527-6543, 1996.
9. Dubuisson Ph., Borde R., Schmechtig C., and Santer R., Surface pressure estimates from satellite data in the oxygen A-band: Applications to the MOS sensor over land, *Journal of Geophysical Research*, Vol 106 (21),27277-27286, 2001.
10. Begni G., Dinguirard M.C., Jackson R.D., and Slater P.N., Absolute calibration of the SPOT-1 HRV cameras, In *Earth Remote Sensing using the Landsat Thematic Mapper and SPOT-sensor Systems (SPIE-660 Proceedings)*: 183p., 1986.
11. Santer R., Gu X.F., Guyot G., Deuzé J.L., Devaux C., Vermote E., and Verbrughe M., SPOT calibration at the La Crau test site - FRANCE, *Remote Sensing of Environment*, Vol 41, 227-237, 1992.
12. Deuzé, J.L., Herman M, and Santer R., Fourier series expansion of the transfer equation in the atmosphere-ocean system, *Journal of Quantitative Spectroscopy & Radiative Transfer*, Vol 41 (6),483-494, 1989.
13. Vermote E.F., Tanré D., Deuzé J.L., Herman M., Morcrette J.J., Second simulation of the satellite signal in the solar spectrum (6S), *Users Guide Version 2.0*, University of Maryland, Greenbelt (MD), and Laboratoire d'Optique Atmosphérique, Lille (France), 218p., 1997.
14. Santer R., Schmechtig C., and Thome K.J., BRDF and surface surround effects on SPOT-HRV vicarious calibration, In *Proceedings of the European Symposium on Aerospace Remote Sensing (SPIE Conference on Image and Signal Processing for Remote Sensing)*, EUROPTO III, Taormina (Italy), September 23-27, 1996.
15. Frouin R., and Gautier C., Calibration of NOAA-7, GOES-5 and GOES-6 VISSR/VAS solar channels, *Remote Sensing of Environment*, Vol 22,73-101, 1987.
16. Nakajima T., and Tanaka M., Algorithms for radiative intensity calculations in moderately thick atmospheres using a truncation approximation, *Journal of Quantitative Spectroscopy & Radiative Transfer*, Vol 40, 51-69, 1988.
17. Nakajima T., and Tanaka M., Matrix formulations for the transfer of solar radiation in a plane-parallel scattering atmosphere, *Journal of Quantitative Spectroscopy & Radiative Transfer*, Vol 35, 13-21, 1986.
18. Hansen J.E., and Travis L., Light scattering in planetary atmospheres, *Space Science Reviews*, Vol 16, 527-610, 1974.
19. Zagolski F., Dilligeard E, Santer R., Perron G., Huot J.P., Radiative transfer code intercomparison for MERIS vicarious calibration, *ABB-BOMEM report (PO-RP-BOM-GS-0031)*, Quebec (Canada), 79p., 2002.
20. Cox C., and Munk W., Measurements of roughness of the sea surface from photographs of the sun glitter, *Journal of Optical Society in America*, Vol 44 (11), 838-888, 1954.
21. Dilligeard, E., Zagolski F., Fischer J., and Santer R., Uncertainties in radiative transfer computation: consequences on the ocean color products, In *Proceedings of the Third International Asia-Pacific Environmental Remote Sensing Symposium (SPIE Conference on Remote Sensing of the Atmosphere, Ocean, Environment, and Space)*, Hangzhou (China), October 23-27, 2002.